ACS OMEGA

http://pubs.acs.org/journal/acsodf

Article

Three-Dimensional Study of Magnetohydrodynamic Natural Convection, Entropy Generation, and Electromagnetic Variables in a Nanofluid Filled Enclosure Equipped with Inclined Fins

Soulayma Gal, Lioua Kolsi, Walid Hassen,* Naim Ben Ali, Nidhal Ben Khedher, and Ali J. Chamkha

Cite This: *ACS Omega* 2022, 7, 12365−12373

Read Online

ACCESS | Metrics & More | Article Recommendations

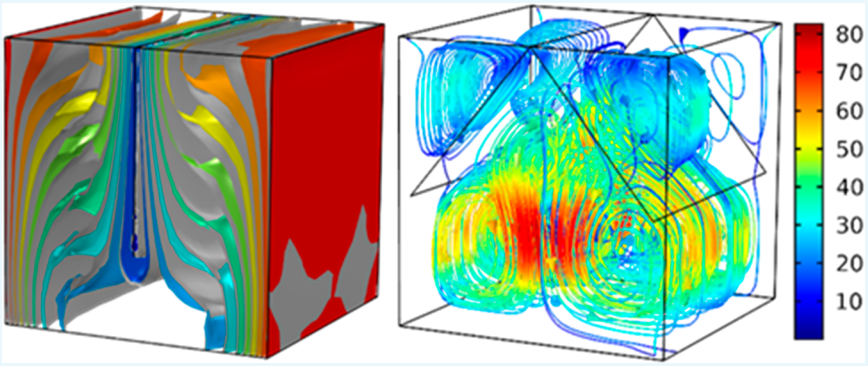

ABSTRACT: This article provides a numerical study on carbon nanotube−water nanofluid convection in a three-dimensional cavity under a magnetic field effect. Two walls are kept at a hot temperature, and the upper and lower horizontal walls are considered adiabatic. As a new configuration, the beneficial effect of using a nanofluid is coupled with the incorporation of cold V-shape obstacle placed in the cubic cavity; in addition, an external magnetic field is applied toward the horizontal *x*-axis direction. The finite element method based on the Galerkin's Weighted Residual technique is used to solve the three-dimensional governing equations. In this paper, the ranges of the parameters used are the Hartmann number, varied from 0 to 100, Rayleigh number from 10^3 to 10^5, nanofluid volume fraction between 0% and 4.5%, and the body V-shaped opening angle varied from 0 to 80°. The effect of the obstacle shape and the added nanoparticle concentration on the flow behaviors, the different instabilities generated, and the heat transfer exchanged were exposed. An enhancement in heat transfer was recorded by increasing the obstacle opening angle and the volume fraction of the carbon nanotubes. Special attention has also been devoted to the calculation of the different kinds of entropy generations.

INTRODUCTION

The control of convective heat transfer in cavities has attracted the interest of many researchers in view of its beneficial technical applications. In some processes such as heat exchangers, thermal engines, furnaces, steam boilers, etc., the aim is to intensify and improve heat transfer. In other processes such as crystal growth, the aim is to minimize convection. Therefore, having a tool for controlling and mastering heat transfer in the same enclosure will be of great interest to engineers. Today, among the vast array of methods available to improve or reduce heat transfer, it was decided in this work to couple three mature techniques: two passive techniques, namely, the use of an adjustable shape obstacle with the addition of nanoparticles, and also an active technique using an external magnetic field. In this context, it should be noted that several studies have focused on enhancing or decreasing heat transfer. Gangawane et al.[1] analyzed the impact of the position and size of a heated triangular body inside a 2D cavity. They showed that there is a direct correlation between Nu_{av} and the position and size of the block in the cavity. Increases of more than 50% were achieved after optimizing the obstacle location and dimension.

Kolsi et al.[2] considered a closed cavity equipped with sharp-edged fins. The 3D calculation of heat transfer and irreversibilities through the generated entropy was performed. The authors were able to find the best fin inclination giving the highest heat exchange and the minimum entropy generation.

Received: February 15, 2022
Accepted: March 17, 2022
Published: March 31, 2022

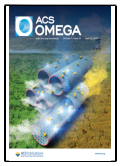

https://doi.org/10.1021/acsomega.2c00923
ACS Omega 2022, 7, 12365−12373

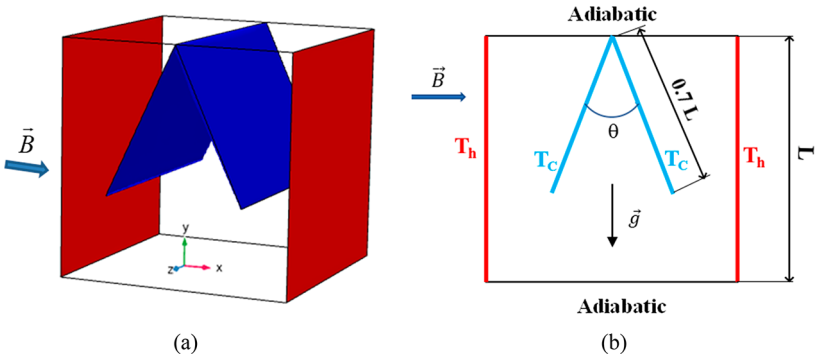

Figure 1. Studied configuration;: (a): 3D geometry and (b) central *xy* plane.

Rathor and Aharwal[3] presented an experimental study to expose the variation in the *Nu* number of several inclined ribs implanted in a rectangular duct representing a solar air heater. The liquid crystal thermography technique was adopted to visualize the temperature distribution. An increase on the order of 229% was recorded.

Du et al.[4] numerically studied the natural convection inside an isolated cavity containing a hot baffle. This cavity, subjected to a magnetic field, contains two diagonally opposed openings located on either side of the vertical walls. The openings allow the creation of a cold fluid flow composed of hybrid nanofluids. The authors were able to demonstrate that the transfer is even better with the inclusion of nanoparticles and, conversely, the use of magnetic fields significantly reduces thermal convection.

The effect of an obstacle[5−8] (square or circular, fixed or rotating) in a lid-driven closed enclosure or of several obstacles[9−11] (of different shapes) in a square cavity subjected to an external magnetic field has been widely treated with the aim of optimizing and improving heat transfer.

Hassen et al.[12] tried to intensify the heat transfer using hot rectangular obstacles of different sizes and at different positions. The enhancement technique was done by creating an electric potential difference between the obstacle and the cavity walls. They were therefore able to set up an electric field that allowed the heat transfer to be improved up to 530%. In another complementary paper,[13] the authors tested the coupling of two intensification techniques: electric field and addition of MWCNT. An improvement of around 43% was recorded.

Xiao et al.[14] proposed the use of inclined baffles to enhance heat exchange performances, in particular the cooling of a solar concentrator focus via thermal oil. The idea is to test three types of baffles which by impact with the fluid will create longitudinal vortices and improve convection. They solved the problem numerically and found that the average global performance and the operating exergy were improved by 0.52% and 0.22%, respectively.

Ajeel et al.[15] numerically simulated the flow and heat transfer through a curved-corrugated pipe filled with a nanofluid in the presence of L-shaped baffles. Their results revealed the development of a vortex flow and an improvement in turbulence as a result of the influence of the wave walls and the baffles. For a specific geometry and amount of the used nanoparticles, an improvement in heat transfer of about 142% was achieved.

Luan and Phu[16] were able to develop correlations for estimating Nu_{av} and a friction coefficient for a solar air heater fitted with tilted obstacles. The correlations were validated experimentally with an error of less than 8%. The authors focused mainly on the estimation of the solar collector efficiency as a function of the tilt angle of the obstacles. The result was that horizontal baffles give the worst efficiency, whereas with baffles sloping between 60° and 120° a high efficiency of up to 62% can be achieved.

The effects of a short, thin fin attached to the hot wall of a partially differentially heated encloser was studied by Torabi et al.[17] The goal of the work is to show how to control the heat transfer by simply adjusting the position of the fin. The authors have shown that it is possible to increase the average *Nu* up to 250%, as it is also possible to decrease it drastically with a careful choice of the fin. Similarly, Mehryan et al.[18] examined the problem of a differentially heated enclosure with a baffle installed on the hot wall. In this study, the baffle is elastically flexible, and the fluid flowing through the cavity can be Newtonian or non-Newtonian. It was proven that the variation of the modulus of elasticity of the baffle has practically no effect on the heat transfer.

Yang et al.[19] investigated the 3D turbulent forced convection in a channel filled with nanofluid. The channel with a constant wall temperature is provided with a rectangular groove. In this study two models were considered: the single-phase and the two-phase (solid−liquid) models treating the nanoparticles and the base fluid separately. The authors mentioned that using grooves can improve the heat transfer by 18.2%.

An experimental study on the heat transfer in a channel equipped with a matrix consisting of a set of 30 V-shaped fins and multiple counter-rotating ribbons was performed by Promvonge.[20] The results revealed that depending on the shape of the ribbons the heat transfer can be enhanced by 63%.

Li et al.[21] studied the natural convection of the alumina dispersed in water mixture. The enclosure is inclined and subjected to a uniform lateral magnetic field. A hot baffle was positioned in the center of the cavity. The results concluded that an increase in the Rayleigh number and the Hartmann number leads to a 350% amplification and a 45% reduction, respectively, in the Nusselt number. Other articles on this topic can be found in the literature.[22,23]

The control of heat transfer by natural convection through the coupling of several passive and active techniques provides good energy efficiency and flexibility of operation of different systems such as electronic equipment, renewable energy technologies, ventilation and heating of buildings, etc. Based on the above literature review and to the best of our knowledge, three-dimensional systems coupling the addition of nanoparticles and a complex shaped obstacle as passive techniques and the application of an external magnetic field as the active technique are almost nonexistent.

https://doi.org/10.1021/acsomega.2c00923
ACS Omega 2022, 7, 12365−12373

This paper is therefore an original work devoted to the understanding of the behavior of the different instabilities that can arise after the application of an external magnetic field on a nanofluid filled enclosure fitted with a complex V-shaped obstacle. The temperature, velocity, entropy, and electric potential fields for different Rayleigh numbers, Hartmann numbers, nanoparticle volume fractions, and obstacle opening angles will be presented, detailed, and discussed.

The remainder of this paper is organized as follows. In Methodology and Mathematical Modeling, the physical model, governing equations, and numerical method are formulated. A subsection presents the Model Verification and Grid Sensitivity Test. The Results and Discussion are presented next. Finally, we end with a Conclusion section.

METHODOLOGY AND MATHEMATICAL MODELING

Physical Problem. A 3D enclosure filled with CNT−water is considered (Figure 1). The left and right walls are kept at a hot

Table 1. Properties of Water (Base Fluid) and CNT (Dispersed Nanoparticles)[29−32]

physical properties	water	CNT
C_P (kJ·kg^{-1}·K^{-1})	4.179	0.425
ρ (kg·m^{-3})	997.1	2600
μ (Pa·s)	10^{-3}	-
k (kW·m^{-1}·K^{-1})	0.613×10^{-3}	6.6
β (K^{-1})	2.1×10^{-6}	16×10^{-7}
σ (Ω^{-1}·m^{-1})	5×10^{-2}	48×10^{-8}

Table 2. Comparison of Nu_{av} with the Findings of Ozoe and Okada[33]

	Nu_{av}	
Ha = 100	present model	4.448
	Ozoe and Okada[33]	4.457
Ha = 200	present model	2.919
	Ozoe and Okada[33]	2.917
Ha = 300	present model	2.254
	Ozoe and Okada[33]	2.251

Table 3. Grid Sensitivity Check for $Ra = 10^5$, $\phi = 0.03$, $Ha = 50$, and $\theta = 40°$

	Nu_{av}	percentage increase	incremental increase
E1: 93175	4.6892	-	-
E2: 169537	4.7812	1.961955	-
E3: 429511	4.9661	5.905058	3.86723
E4: 1227850	5.01	6.841252	0.883993

temperature, while two cold fins are attached to the top wall. The flow is considered incompressible under the dual effects of buoyancy force based on the Boussinesq approximation and the Lorentz force generated by the applied magnetic field in the "x" direction ($\vec{B} = B_0\vec{e}_x$).

The volume fraction of the nanofluid never exceeds 5%, so it can be considered that the mixture is homogeneous and single-phase.

Governing Equations. Under the above-mentioned assumptions, the governing equations are given as

$$\nabla\cdot\vec{V'} = 0 \tag{1}$$

$$\frac{\partial\vec{V'}}{\partial t'} + (\vec{V'}\cdot\vec{\nabla})\vec{V'} = -\frac{1}{\rho_{nf}}\vec{\nabla}P' + \frac{1}{\rho_{nf}}(\vec{J'}\times\vec{B'}) + \nu\Delta\vec{V'} - \beta_f(T' - T'_c)\vec{g} \tag{2}$$

$$\frac{\partial T'}{\partial t'} + \vec{V'}\cdot\nabla T' = \alpha_{nf}\Delta T' \tag{3}$$

$$\vec{J'} = \sigma_{nf}(\vec{\nabla}\phi' + \vec{V}'\times\vec{B'}) \quad \text{with} \quad \vec{E} = -\vec{\nabla}\phi' \tag{4}$$

$$\nabla\cdot\vec{J}' = 0 \tag{5}$$

The dimensionless variables are chosen as

$$t = \frac{t'}{L'^2/\alpha}; (x,y,z) = \frac{(x,y,z)'}{L'}; (V_x,V_y,V_z) = \frac{(V_x,V_y,V_z)'}{\alpha/L'}; P = \frac{P'}{\rho(\alpha/L')}; \vec{J} = \frac{\vec{J'}}{\sigma\cdot V_0\cdot B_0}; \vec{B} = \frac{\vec{B}'}{B_0}; \phi = \frac{\phi'}{l\cdot V_0\cdot B_0}; \text{and } T = \frac{(T' - T_c')}{(T_h' - T_c')}$$

Thus, the governing equations becomes as follows:

$$\nabla\cdot\vec{V} = 0 \tag{6}$$

$$\frac{\partial\vec{V}}{\partial t} + (\vec{V}\cdot\vec{\nabla}\vec{V}) = -\vec{\nabla}P + \frac{\sigma_{nf}\rho_f}{\sigma_n\rho_{nf}}Ha^2Pr(\vec{J}\times\vec{B}) + Pr\left(\frac{\nu_{nf}}{\nu_f}\right)\Delta\vec{V} + \left(\frac{\beta_{nf}}{\beta_f}\right)RaPr\vec{T}_g \tag{7}$$

$$\frac{\partial T}{\partial t} + \vec{V}\cdot\nabla T = \frac{\alpha_{nf}}{\alpha_f}\nabla^2 T \tag{8}$$

$$\vec{J} = -\vec{\nabla}\phi + \vec{V}\times\vec{e}_B \tag{9}$$

$$\vec{\nabla}^2\phi = \vec{\nabla}\cdot(\vec{V}\times\vec{B}) \tag{10}$$

with

$$Pr = \frac{\nu_f}{\alpha_f}; Ra = \frac{g\cdot\beta_f\cdot\Delta T\cdot l^3}{\nu_f\cdot\alpha_f}; \text{and } Ha = B_0L\sqrt{\frac{\sigma}{\rho_f\nu_f}}$$

Boundary conditions are stated as

- $x = 0; x = 1; T = T_h; u = v = w = 0$
- $y = z = 0; y = z = l; \frac{\partial T}{\partial n} = 0; u = v = w = 0$
- On obstacle: $T = T_c; u = v = w = 0; \frac{\partial\phi}{\partial n} = 0; \vec{J}\cdot\vec{n} = 0$
- $\frac{\partial\phi}{\partial n} = 0$ at all walls
- $\vec{J}\cdot\vec{n} = 0$ on all walls

Considering the MHD effect, the entropy generation is expressed as

https://doi.org/10.1021/acsomega.2c00923
ACS Omega 2022, 7, 12365−12373

$$S'_{gen} = \left\{\frac{k_{nf}}{T_0^2}\left[\left(\frac{\partial T'}{\partial x'}\right)^2 + \left(\frac{\partial T'}{\partial y'}\right)^2 + \left(\frac{\partial T'}{\partial z'}\right)^2\right]\right\} + \frac{\mu_{nf}}{T_0}\left\{2\left[\left(\frac{\partial V'_x}{\partial x'}\right)^2 + \left(\frac{\partial V'_y}{\partial y'}\right)^2 + \left(\frac{\partial V'_z}{\partial z'}\right)^2\right] + \left(\frac{\partial V'_y}{\partial x'} + \frac{\partial V'_x}{\partial y'}\right)^2 + \left(\frac{\partial V'_z}{\partial y'} + \frac{\partial V'_y}{\partial z'}\right)^2 + \left(\frac{\partial V'_x}{\partial z'} + \frac{\partial V'_z}{\partial x'}\right)^2\right\} + \frac{1}{T_0}\frac{1}{\sigma_{nf}}(J'^2_x + J'^2_y + J'^2_z) \quad (11)$$

Using the above-mentioned dimensionless variable, the local generated entropy (N_s) becomes

$$N_s = \frac{k_{nf}}{k_f}\left[\left(\frac{\partial T}{\partial x}\right)^2 + \left(\frac{\partial T}{\partial y}\right)^2 + \left(\frac{\partial T}{\partial z}\right)^2\right] + \varphi_s\frac{\mu_{nf}}{\mu_f}\left\{2\left[\left(\frac{\partial V_x}{\partial x}\right)^2 + \left(\frac{\partial V_y}{\partial y}\right)^2 + \left(\frac{\partial V_z}{\partial z}\right)^2\right] + \left[\left(\frac{\partial V_y}{\partial x} + \frac{\partial V_x}{\partial y}\right)^2 + \left(\frac{\partial V_z}{\partial y} + \frac{\partial V_y}{\partial z}\right)^2 + \left(\frac{\partial V_x}{\partial z} + \frac{\partial V_z}{\partial x}\right)^2\right]\right\} + I_s\frac{\mu_f}{\mu_{nf}} + \frac{\sigma_{nf}}{\sigma_f}Ha^2(J_x^2 + J_y^2 + J_z^2) \quad (12)$$

with $I_s = \left(\frac{\alpha_f}{l\Delta T}\right)^2 T_0$ as the irreversibility coefficient.

The total generated entropy is expressed as

$$S_{tot} = \int_v N_s\, dv = \int_v (N_{s-th} + N_{s-fr} + N_{s-m})\, dv = S_{th} + S_{fr} + S_m \quad (13)$$

The Bejan number is

$$Be = \frac{S_{th}}{S_{th} + S_{fr} + S_m} \quad (14)$$

The local and average Nusselt numbers are

$$Nu = \left(\frac{k_{nf}}{k_f}\right)\left(\left.\frac{\partial T}{\partial x}\right|_{x=0} + \left.\frac{\partial T}{\partial x}\right|_{x=1}\right) \quad (15)$$

and

$$Nu_{av} = \int_0^1\int_0^1 Nu\, dy\, dz \quad (16)$$

The effective properties (Table 1) of the CNT−nanofluid are[24−29]

$$\rho_{nf} = (1-\phi)\rho_f + \phi\rho_s \quad (17)$$

$$C_{p,nf} = \frac{(1-\phi)(\rho_f C_{p,f}) + \phi(\rho_{CNT} C_{p,CNT})}{\rho_{nf}} \quad (18)$$

$$\beta_{nf} = \frac{(1-\phi)(\rho_f\beta_f) + \phi(\rho_{CNT}\beta_{CNT})}{\rho_{nf}} \quad (19)$$

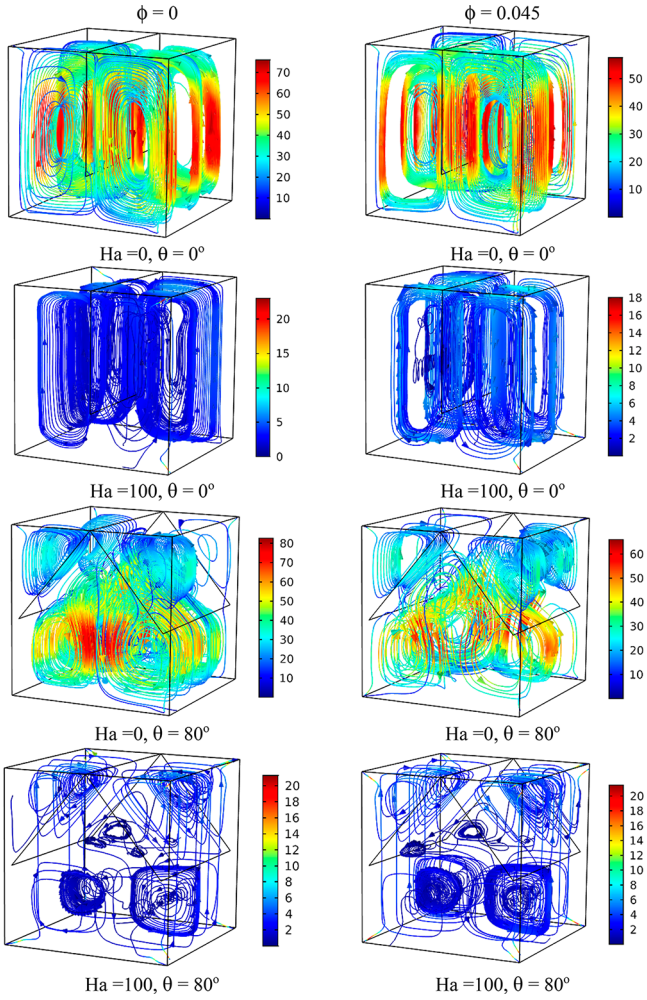

Figure 2. Flow field for different *Ha* numbers and inclination angle of the fins for $Ra = 10^5$.

$$\mu_{nf} = \mu_f(1 + a\phi + b\phi^2) \quad (20)$$

With $a = 13.5$ and $b = 904.4$ for tube shaped nanoparticles (Hamilton and Crosser model),

$$k_{nf} = k_f\frac{(1-\phi) + 2\phi\frac{k_{CNT}}{k_{CNT}-k_f}\ln\frac{k_{CNT}+k_f}{2k_f}}{(1-\phi) + 2\phi\frac{k_f}{k_{CNT}-k_f}\ln\frac{k_{CNT}+k_f}{2k_f}} \quad (21)$$

$$\sigma_{nf} = \sigma_f\left[1 + \frac{3\cdot\varphi\cdot\left(\frac{\sigma_s}{\sigma_f} - 1\right)}{\left(\frac{\sigma_s}{\sigma_f} + 2\right) - \varphi\cdot\left(\frac{\sigma_s}{\sigma_f} - 1\right)}\right] \quad (22)$$

Numerical Method. The FEM method based on the Galerkin's Weighted Residual technique is employed to solve the set of the dimensionless governing eqs 6−10. The Lagrange polynomials are expressed as

$$g = \sum_{j=1}^{Ns}\Omega_j^s G_j$$

- Ω: shape function
- *G*: values at the nodes of the elements.
- Time dependent parts are treated by the backward differentiation formula (BDF)

https://doi.org/10.1021/acsomega.2c00923
ACS Omega 2022, 7, 12365−12373

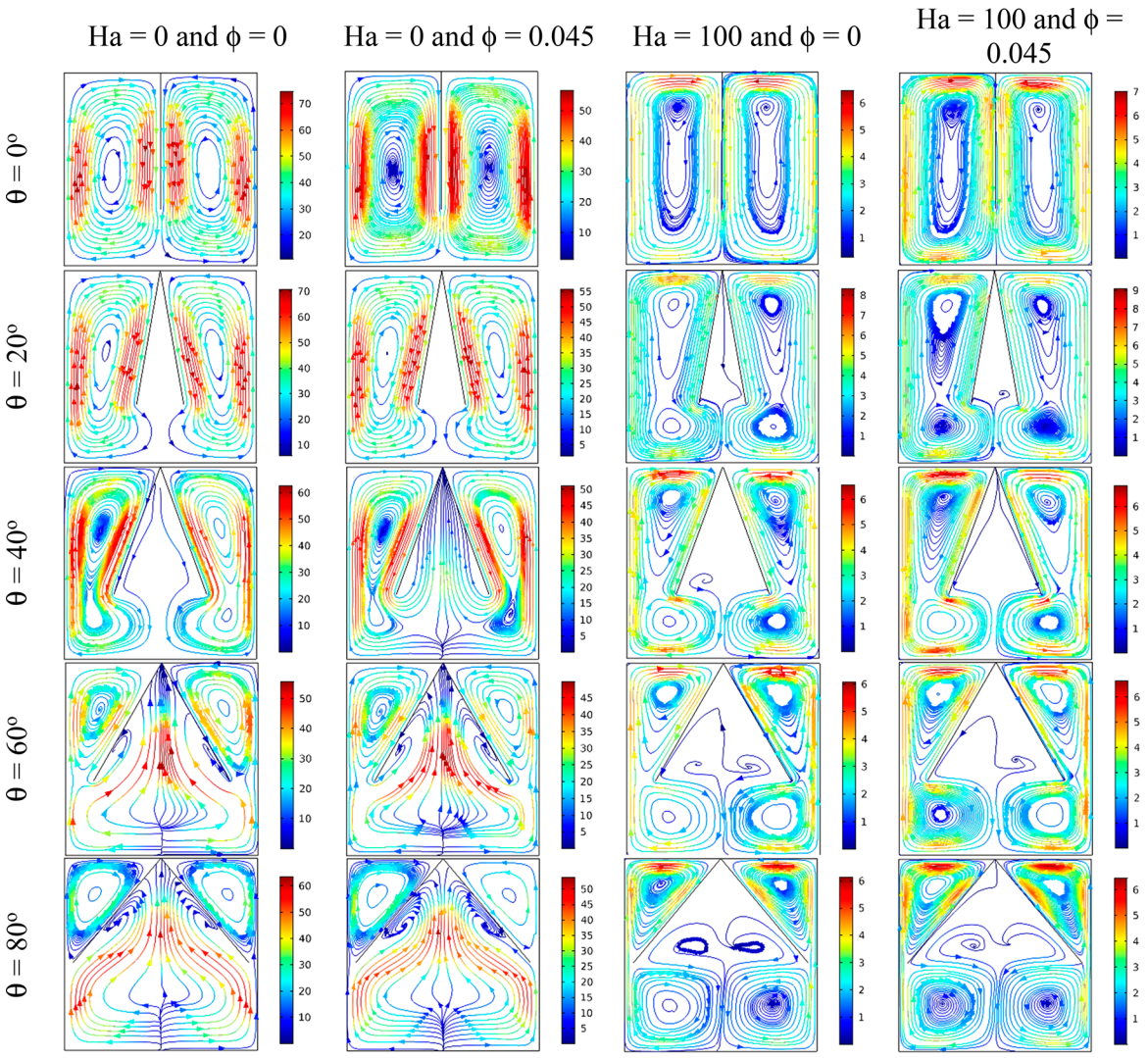

Figure 3. Effects of fin inclination angle for different nanoparticle volume fractions, *Ha* numbers, and inclination angles for $Ra = 10^5$.

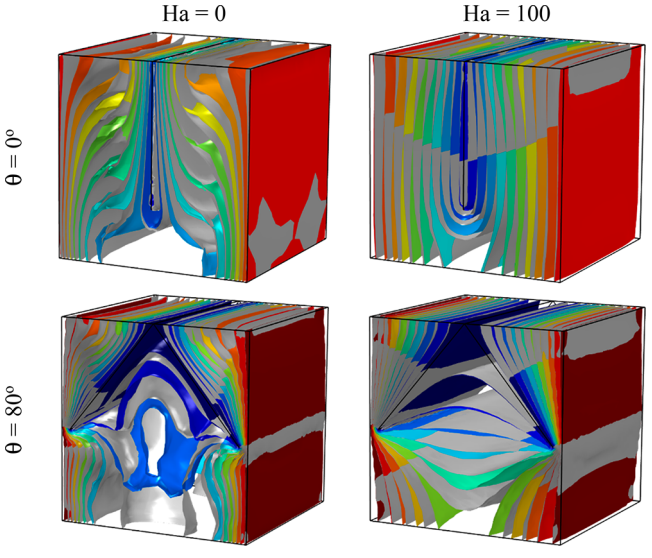

Figure 4. Temperature distribution for $Ra = 10^5$. Colors ($\phi = 0.045$) and gray ($\phi = 0$) indicate different angles between the fins.

- The convergence criterion is $\left|\frac{\Gamma^{n+1} - \Gamma^{n}}{\Gamma^{n+1}}\right| \leq 10^{-6}$

Model Verification and Grid Sensitivity Test. The verification of the present model (Table 2) is performed by comparison with the 3D findings of Ozoe and Okada.[33] The comparison shows a good agreement between the results.

To check the grid sensitivity (Table 3), the results of Nu_{av} are compared for three mesh element numbers, namely, E1, E2, E3, and E4, for $Ra = 10^5$, $\phi = 0.03$, $Ha = 50$, and $\theta = 40°$. The difference between the result of the mesh E3 and and that of mesh E4 is only 0.88%; thus, in order to get accurate results while saving the computation time, the mesh number E3 is opted for in all the numerical executions.

RESULTS AND DISCUSSION

Figure 2 illustrates the 3D flow structure for two the values of θ in the absence and presence of the magnetic field. From this figure it can be noticed that the flow structure is highly affected by the angle between the obstacles. In fact, a multivortex regime is created just by varying the θ angle from 0 to 80°. However, when the baffle was fixed at $\theta = 0°$, the cavity gets divided into two parts, and each section behaves in one vortex; when it is fixed at $\theta = 80°$, the flow becomes multicellular. In the absence of the magnetic field, the addition of a CNT ($\phi = 0.045$) reduces the flow intensity by 23.33% for $\theta = 0$ and 28.12% for $\theta = 80°$.

https://doi.org/10.1021/acsomega.2c00923
ACS Omega 2022, 7, 12365−12373

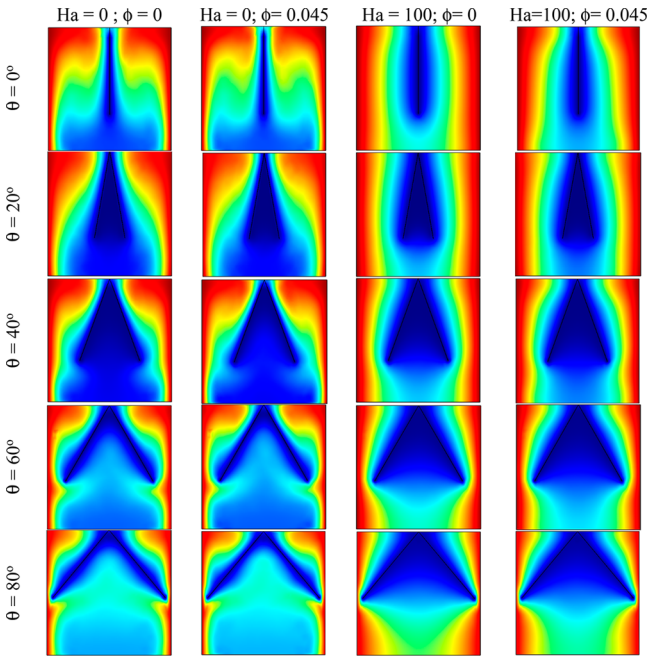

Figure 5. Temperature field at the $z = 0.5$ plane for $Ra = 10^5$ at different nanoparticle volume fractions and inclination angles of the fins.

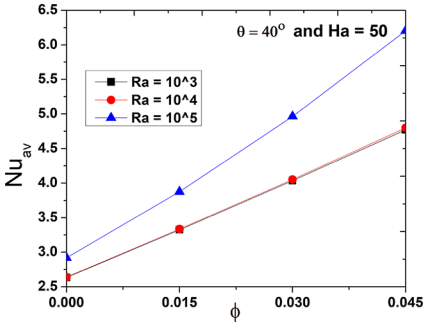

Figure 6. Nu_{av} versus CNT volume fraction for various Ra values at $\theta = 40^\circ$ and $Ha = 50$.

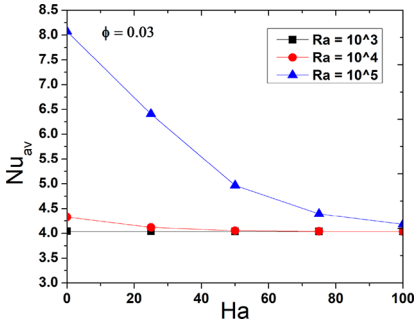

Figure 7. Nu_{av} versus Hartman number for various Ra values at $\phi = 0.03$.

This is due to the increase of the viscous dissipations. On the other hand, for $Ha = 100$, the flow intensity is slightly reduced 27.8% for $\theta = 0$ and remains quasi-constant for $\theta = 80^\circ$. The magnetic field has a flow damping effect due to the generated Lorentz force. It is also to be mentioned that, for all the cases, the flow has a 3D character with a complex structure, and in addition to the main flow, a transversal flow occurs toward the z-axis.

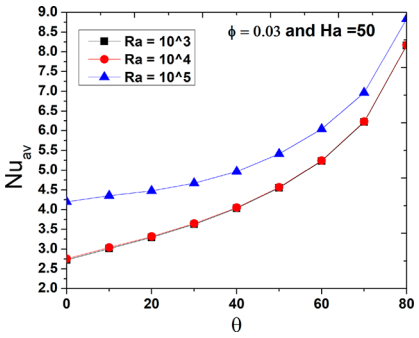

Figure 8. Nu_{av} versus the inclination between the fins for $Ha = 50$, $\phi = 0.03$, and various values of Ra.

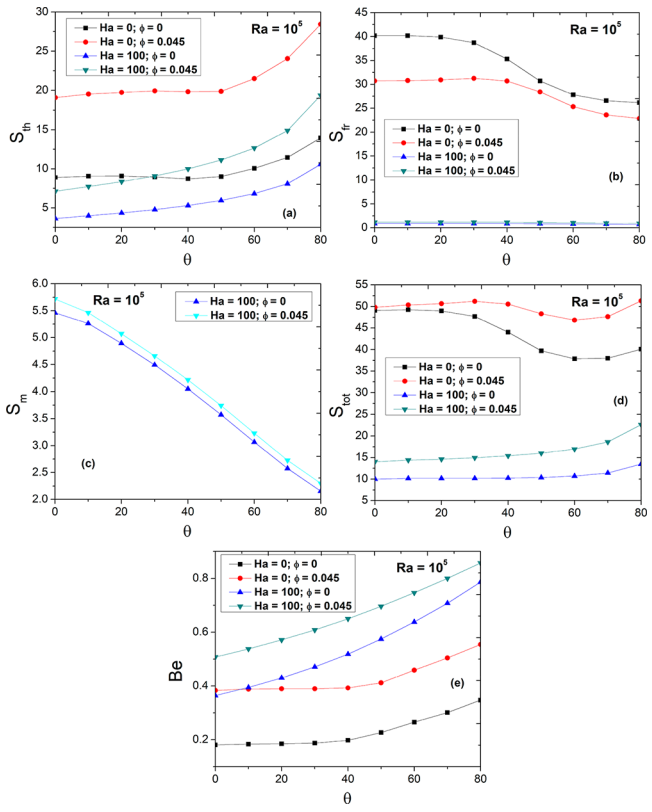

Figure 9. Effect of θ on the entropy generation for $Ra = 10^5$: (a) thermal, (b) viscous, (c) magnetic, (d) total, and (e) Bejan Number.

Thus, Figure 3 is presented for a better understanding of the flow behavior and cellular behavior.

Figure 3 illustrates the effects of the angle between the fins on the main central flow structure.

It is to be mentioned that, for all the considered cases, the addition of CNTs reduces the flow intensity due to the increase of the viscosity. As an illustration, for $Ha = 0$, the addition of nanoparticles causes a reduction of the magnitude of the velocity by about 35% for all the cases. Also, the application of the magnetic field causes a Lorentz force that opposes the thermal buoyancy and induces a square shaped flow near the walls.

For $\theta = 0$, the flow is composed of two counter-rotating vortexes that rise up by applying the magnetic field. The increase of the angle between the cold fins causes the apparition of a multivortex structure, especially for higher CNT volume fraction and Hartman numbers.

https://doi.org/10.1021/acsomega.2c00923
ACS Omega 2022, 7, 12365−12373

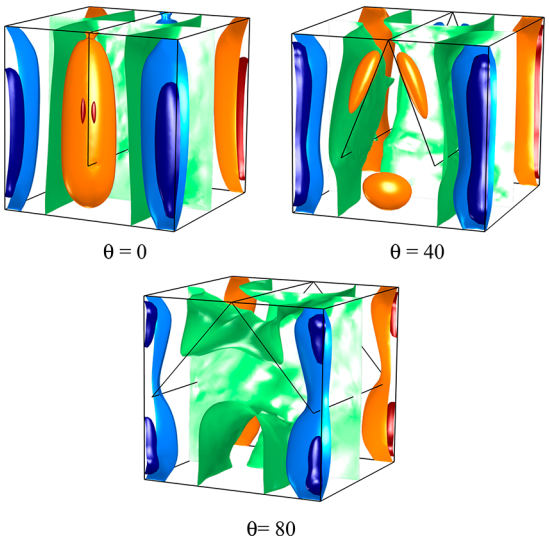

Figure 10. Electrical Potential for $Ra = 10^5$, $Ha = 50$, and $\phi = 0.045$.

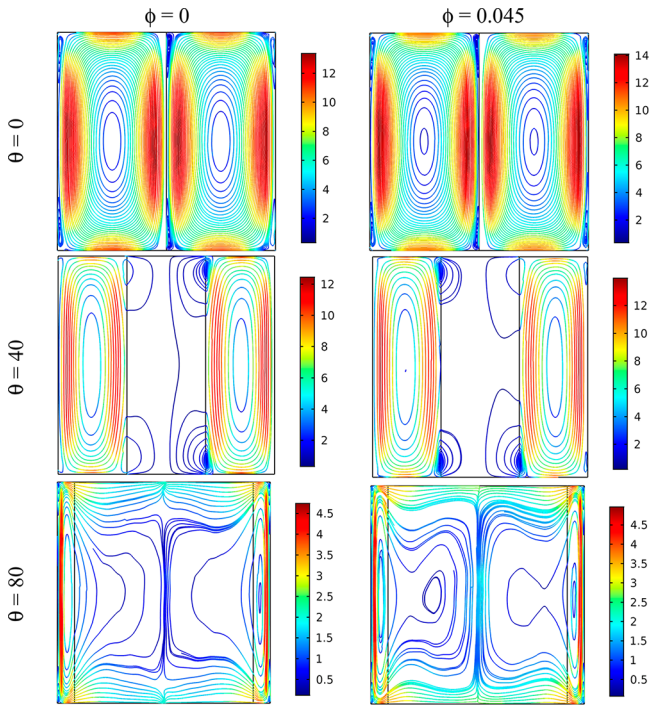

Figure 11. Current density at the central *xz* plane for $Ra = 10^5$ and $Ha = 50$.

Figures 4 and 5 present the temperature iso-surfaces and the temperature fields, respectively, for $Ra = 10^5$ at different angles between the fins. In the absence of the magnetic effect and due to the intensity of the flow, distortions and vertical stratifications of the iso-surfaces of temperature are encountered. These distortions and vertical stratifications become more important by adding the CNT. The magnetic effect reduces the distortions; the iso-surfaces of the temperature become parallel to the cold fins, and the temperature field becomes similar to that of a purely conductive regime due to the damping effect of the induced Lorentz force. It is also noticed that the temperature gradients close to the active walls are increased by adding the CNT and reduced by increasing Hartman number. This finding means that the heat transfer is enhanced by the increase of the nanoparticle's concentration and damped by the presence of the magnetic field.

Figure 6 illustrates the effect of the CNT volume fraction on the heat transfer rate for $\theta = 40°$ and $Ha = 50$. The increase of Ra is obviously found to increase Nu_{av} due to the increase of the buoyancy forces. The addition of nanoparticles ameliorates the properties of the nanofluid and consequently enhances the heat transfer. In fact, Nu_{av} is approximatively doubled by increasing the CNT volume fractions from 0 to 0.045.

The effect of the applied external magnetic field on Nu_{av} is presented in Figure 7. For all the considered Ra values, Nu_{av} is significatively reduced by the applied magnetic field. For example, for $Ra = 10^5$ a reduction of about 43% occurs. This reduction is justified by the induced Lorentz force that opposes the convective flow and reduces the temperature gradient close to the active walls.

As presented in Figure 8 and in opposition with the effect of Ha, the increase of the angle between the fins causes a considerable enhancement of the heat transfer rate. In fact, the Nu_{av} number is doubled by increasing the angle from 0 to 80°. This is due to the fact that the hot and cold surfaces become closer, which causes the intensification of the thermal buoyancy in the created tight regions.

The effect of the angle between the fins on the irreversibility productions is depicted in Figure 9, for $Ra = 10^5$ and various Ha and ϕ values. It is to be mentioned that the irreversibility coefficient is fixed at $I_s = 10^{-4}$. The angle between the fins has different effects on the evaluated types of irreversibility. In fact, it increases the thermal entropy and decreases both the viscous and magnetic entropy generations. The increase of the thermal entropy production is due to an increase of the temperature gradients when the cold fins come close to the hot walls, while the viscous entropy generation decreases due to the opposition of fins to the flow when the angle between the fins is higher. The variation of the total entropy generation has different behaviors in the presence and in the absence of the magnetic field. In fact, it is decreasing and then increasing for $Ha = 0$ and is increasing for $Ha = 100$. It is also to be mentioned that the addition of CNT nanoparticles causes the increase of all the types of entropies and, in opposition, the application of the magnetic field reduces them. The variation of the Be number is also monotone, indicating that the increase of the angle between the fins favors the thermal entropy generation compared to the other kinds of entropies.

Figure 10 presents the iso-surface of the electrical potential for $Ra = 10^5$, $Ha = 50$, and $\phi = 0.045$ and various angles between the fins. The maximum and minimum values of the electrical potential are located at the corner and are mainly null in the core region of the cavity. The increase of the angle causes a distortion of these iso-surfaces.

Figure 11 illustrates the current density at the central *xz*-plane for $Ra = 10^5$ and $Ha = 50$. It is noticed that the current lines are closed due to electrical insulation of the walls with the apparition of counter-rotative cells at the corners. This is due to the dominance of the electrical potential $(-\vec{\nabla}_{\varphi})$ compared to the induced electrical current $(\vec{V} \times \vec{e}_B)$. The increases of the angle between the fins reduce the size of the principal cells of the current density. It is also noticed that the addition of CNT causes an increase in the magnitude of the current density due to the enhancement of the electrical conductivity.

https://doi.org/10.1021/acsomega.2c00923
ACS Omega 2022, 7, 12365−12373

CONCLUSION

A 3D numerical simulation on the MHD convective heat transfer of CNTs dispersed in water in a cubic cavity equipped with two inclined fins is performed using the FEM. The main conclusions can be summarized as follows.

- The use of nanoparticles can enhance the heat transfer rate by 100% and augments the entropy production by 30%.
- The increase of the angle between the fins causes considerable changes in the flow and temperature fields.
- The application of the magnetic field allows a control of the flow and the heat transfer. A reduction of about 100% in the Nusselt number was recorded just by varying *Ha* from 0 to 100.
- The variation of the fin inclination from 0 to 80% intensifies the heat transfer by 218%.
- The electromagnetic variables are affected by the presence of the fins.
- For a strong magnetic field (Ha = 100), the viscous entropy is destroyed at the expense of the magnetic entropy.
- Increasing the fin angle decreases the viscous entropy but increases the thermal and magnetic entropy.
- The use of CNT reduces the flow intensity and causes an augmentation of the magnitude of the electrical current density.

AUTHOR INFORMATION

Corresponding Author

Walid Hassen − *Laboratory of Metrology and Energy systems, Monastir, University of Monastir, 5000 Monastir, Tunisia;* orcid.org/0000-0002-6779-2335; Email: hassen.walid@gmail.com

Authors

Soulayma Gal − *Laboratory of Metrology and Energy systems, Monastir, University of Monastir, 5000 Monastir, Tunisia*

Lioua Kolsi − *Mechanical Engineering Department, College of Engineering, University of Ha'il, 81451 Ha'il City, Saudi Arabia*

Naim Ben Ali − *Department of Industrial Engineering, College of Engineering, University of Ha'il, 81451 Ha'il City, Saudi Arabia*

Nidhal Ben Khedher − *Mechanical Engineering Department, College of Engineering, University of Ha'il, 81451 Ha'il City, Saudi Arabia*

Ali J. Chamkha − *Faculty of Engineering, Kuwait College of Science and Technology, Doha District 35004, Kuwait*

Complete contact information is available at: https://pubs.acs.org/10.1021/acsomega.2c00923

Notes

The authors declare no competing financial interest.

ACKNOWLEDGMENTS

This research has been funded by Scientific Research Deanship at University of Ha'il, Saudi Arabia, through Project Number RG-21 035.

NOMENCLATURE

$\vec{B}$	dimensionless magnetic field ($= \vec{B'} / B_0$)
Be	Bejan number
C_p	specific heat capacity, kJ·kg^{-1}·K^{-1}
$\vec{e_B}$	direction of the magnetic field
$\vec{E}$	dimensionless electric field
$\vec{F}$	dimensionless Lorentz force
$\vec{g}$	gravitational acceleration, m·s^{-2}
Ha	Hartmann number
I_S	irreversibility coefficient
$\vec{J}$	dimensionless density of electrical current
K	thermal conductivity, kW·m^{-1}·K^{-1}
Nu	Nusselt number
N_S	dimensionless local generated entropy
P	dimensionless pressure
Pr	Prandtl number
Ra	Rayleigh number
S'_{gen}	entropy generation, J·K^{-1}
S_{tot}	dimensionless total generated entropy
T	dimensionless temperature
t	dimensionless time
$\vec{V}$	dimensionless velocity vector
x, y, z	dimensionless Cartesian coordinates

Greek Characters

α	thermal diffusivity, m^2·s^{-1}
β	thermal expansion coefficient, K^{-1}
μ	dynamic viscosity, Pa·s
ν	kinematic viscosity, m^2·s^{-1}
ρ	density of the fluid, kg·m^{-3}
σ	electric conductivity, Ω^{-1}·m^{-1}

Subscripts

av	average
c	cold
fr	friction
h	hot
m	magnetic
nf	nanofluid
p	solid particle
th	thermal

ABBREVIATIONS

BDF	backward differentiation formula
CNTs	carbon nanotubes
FEM	finite element method
MHD	magnetohydrodynamics
MWCNTs	multiwall carbon nanotubes

REFERENCES

(1) Gangawane, K. M.; Oztop, H. F.; Abu-Hamdeh, N. Mixed convection characteristic in a lid-driven cavity containing heated triangular block: Effect of location and size of block. *Int. J. Heat Mass Transfer* **2018**, *124*, 860−875.

(2) Kolsi, L.; Oztop, H. F.; Abu-Hamdeh, N.; Alghamdi, A.; Naceur Borjini, M. Three dimensional analysis of natural convection and entropy generation in a sharp edged finned cavity. *Alexandria Eng. J.* **2016**, *55*, 991−1004.

(3) Rathor, Y.; Aharwal, K. R. Heat transfer enhancement due to a staggered element using liquid crystal thermography in an inclined discrete rib roughened solar air heater. *Int. Commun. Heat Mass Transfer* **2020**, *118*, 104839.

(4) Du, R.; Gokulavani, P.; Muthtamilselvan, M.; Al-Amri, F.; Abdalla, B. Influence of the Lorentz force on the ventilation cavity having a centrally placed heated baffle filled with the Cu-Al_2O_3-H_2O hybrid nanofluid. *Int. Commun. Heat Mass Transfer* **2020**, *116*, 104676.

(5) Bansal, S.; Chatterjee, D. Magneto-convective transport of nanofluid in a vertical lid-driven cavity including a heat-conducting

https://doi.org/10.1021/acsomega.2c00923
ACS Omega 2022, 7, 12365−12373

rotating circular cylinder. *Numer. Heat Transfer, Part A* **2015**, *68*, 411−431.
(6) Ray, S.; Chatterjee, D. MHD mixed convection in a lid-driven cavity including heat conducting circular solid object and corner heaters with Joule heating. *Int. Commun. Heat Mass Transfer* **2014**, *57*, 200−207.
(7) Ray, S.; Chatterjee, D. MHD mixed convection in a lid-driven cavity including heat conducting solid object and corner heaters with Joule heating. *Numer. Heat Transfer, Part A* **2014**, *66*, 530−550.
(8) Chatterjee, D. MHD mixed convection in a lid-driven cavity including a heated source. *Numer. Heat Transfer, Part A* **2013**, *64*, 235−254.
(9) Chatterjee, D.; Mishra, R. Numerical investigation of transient magnetohydrodynamic mixed convection in a ventilated cavity containing two heated circular cylinders. *Heat Transfer Eng.* **2018**, *39*, 1052−1066.
(10) Chatterjee, D.; Kumar Gupta, S. Magnetohydrodynamic natural convection in a square enclosure with four circular cylinders positioned at different rectangular locations. *Heat Transfer Eng.* **2017**, *38*, 1449−1465.
(11) Chatterjee, D.; Halder, P. MHD mixed convective transport in square enclosure with two rotating circular cylinders. *Numer. Heat Transfer, Part A* **2014**, *65*, 802−824.
(12) Hassen, W.; Kolsi, L.; Ghachem, K.; Almeshaal, M. A.; Maatki, C.; Borjini, M. N. Numerical investigation of electro-thermo-convection in a square enclosure with incorporated hot solid body. *J. Therm. Anal. Calorim.* **2021**, *143*, 2647−2661.
(13) Hassen, W.; Kolsi, L.; Mohammed, H. A.; Ghachem, K.; Sheikholeslami, M.; Almeshaal, M. A. Transient electrohydrodynamic convective flow and heat transfer of MWCNT-Dielectric nanofluid in a heated enclosure. *Phys. Lett. A* **2020**, *384*, 126736.
(14) Xiao, H.; Liu, P.; Liu, Z.; Liu, W. Performance analyses in parabolic trough collectors by inserting novel inclined curved-twisted baffles. *Renewable Energy* **2021**, *165*, 14−27.
(15) Ajeel, R. K.; Sopian, K.; Zulkifli, R. Thermal-hydraulic performance and design parameters in a curved-corrugated channel with L-shaped baffles and nanofluid. *J. Energy Storage* **2021**, *34*, 101996.
(16) Luan, N. T.; Phu, N. M. Thermohydraulic correlations and exergy analysis of a solar air heater duct with inclined baffles. *Case Stud. Therm. Eng.* **2020**, *21*, 100672.
(17) Torabi, M.; Keyhani, A.; Peterson, G. P. A comprehensive investigation of natural convection inside a partially differentially heated cavity with a thin fin using two-set lattice Boltzmann distribution functions. *Int. J. Heat Mass Transfer* **2017**, *115*, 264−277.
(18) Shahabadi, M.; Mehryan, S. A. M.; Ghalambaz, M.; Ismael, M. Controlling the natural convection of a non-Newtonian fluid using a flexible fin. *Appl. Math. Modell.* **2021**, *92*, 669−686.
(19) Yang, Y. T.; Tang, H. W.; Zeng, B. Y.; Wu, C. H. Numerical simulation and optimization of turbulent nanofluids in a three-dimensional rectangular rib-grooved channel. *Int. Commun. Heat Mass Transfer* **2015**, *66*, 71−79.
(20) Promvonge, P. Thermal performance in square-duct heat exchanger with quadruple V-finned twisted tapes. *Appl. Therm. Eng.* **2015**, *91*, 298−307.
(21) Li, Z.; Hussein, A. K.; Younis, O.; Afrand, M.; Feng, S. Natural convection and entropy generation of a nanofluid around a circular baffle inside an inclined square cavity under thermal radiation and magnetic field effects. *Int. Commun. Heat Mass Transfer* **2020**, *116*, 104650.
(22) Arif, S.; Taweekun, J.; Ali, H. M.; Yanjun, D. A. I.; Ahmed, A. Feasibility study and economic analysis of grid connected solar powered net zero energy building (NZEB) of shopping mall for two different climates of Pakistan and Thailand. *Case Stud. Therm. Eng.* **2021**, *26*, 101049.
(23) Akram, M. A.; Khushnood, S.; Tariq, S. L.; Nizam, L. A.; Ali, H. M. The effect of grid generated turbulence on the fluidelastic instability response in parallel triangular tube array. *Ann. Nucl. Energy* **2021**, *158*, 108245.
(24) Abu-Nada, E.; Chamkha, A. J. Mixed convection flow in a lid-driven inclined square enclosure filled with a nanofluid. *Eur. J. Mech. B/Fluids* **2010**, *29*, 472−482.
(25) Basak, T.; Roy, S.; Pop, I. Heat flow analysis for natural convection within trapezoidal enclosures based on heatline concept. *Int. J. Heat Mass Transfer* **2009**, *52*, 2471−2483.
(26) Imtiaz, M.; Hayat, T.; Alsaedi, A.; Ahmad, B. Convective flow of carbon nanotubes between rotating stretchable disks with thermal radiation effects. *Int. J. Heat Mass Transfer* **2016**, *101*, 948−957.
(27) Selimefendigil, F.; Oztop, H. F. Control of natural convection in a CNT-water nanofluid filled 3D cavity by using an inner T-shaped obstacle and thermoelectric cooler. *Int. J. Mech. Sci.* **2020**, *169*, 105104.
(28) Hamilton, R. L.; Crosser, O. K. Thermal conductivity of heterogeneous two-component systems. *Ind. Eng. Chem. Fundam.* **1962**, *1*, 187−191.
(29) Kolsi, L.; Alrashed, A. A.; Al-Salem, K.; Oztop, H. F.; Borjini, M. N. Control of natural convection via inclined plate of CNT-water nanofluid in an open sided cubical enclosure under magnetic field. *Int. J. Heat Mass Transfer* **2017**, *111*, 1007−1018.
(30) Benos, L. T.; Karvelas, E. G.; Sarris, I. E. A theoretical model for the magnetohydrodynamic natural convection of a CNT-water nanofluid incorporating a renovated Hamilton-Crosser model. *Int. J. Heat Mass Transfer* **2019**, *135*, 548−560.
(31) Al-Rashed, A. A.; Kalidasan, K.; Kolsi, L.; Aydi, A.; Malekshah, E. H.; Hussein, A. K.; Kanna, P. R. Three-dimensional investigation of the effects of external magnetic field inclination on laminar natural convection heat transfer in CNT−water nanofluid filled cavity. *J. Mol. Liq.* **2018**, *252*, 454−468.
(32) Job, V. M.; Gunakala, S. R. Unsteady MHD free convection nanofluid flows within a wavy trapezoidal enclosure with viscous and Joule dissipation effects. *Numer. Heat Transfer, Part A* **2016**, *69*, 421−443.
(33) Ozoe, H.; Okada, K. The effect of the direction of the external magnetic field on the three-dimensional natural convection in a cubical enclosure. *Int. J. Heat Mass Transfer* **1989**, *32*, 1939−1954.

https://doi.org/10.1021/acsomega.2c00923
ACS Omega 2022, 7, 12365−12373